Micro-engineered Nanowire Electron Source for Atomic Resolution Imaging

Han Zhang (zhang.han@nims.go.jp)
National Institute for Materials Science

Yu Jimbo
JEOL Ltd.

Akira Niwata
JEOL Ltd.

Akihiro Ikeda
JEOL Ltd.

Akira Yasuhara
JEOL Ltd.

Ovidiu Cretu
National Institute for Materials Science

Koji Kimoto
National Institute for Materials Science https://orcid.org/0000-0002-3927-0492

Takeshi Kasaya
National Institute for Materials Science

Hideki Miyazaki
National Institute for Materials Science https://orcid.org/0000-0003-4152-1171

Naohito Tsujii
National Institute for Materials Science

Hongxin Wang
National Institute for Materials Science

Yasushi Yamauchi
National Institute for Materials Science

Daisuke Fujita
National Institute for Materials Science https://orcid.org/0000-0001-7025-0265

Shin-ichi Kitamura

Hironobu Manabe
JEOL Ltd.

Article

Keywords: Size Tunability, Chemical Versatility, Nanometric Emission Volume, Sub-degree Angular Deviation, Collimated Electron Beam, Lateral and Angular Alignment

Posted Date: April 26th, 2021

DOI: https://doi.org/10.21203/rs.3.rs-445131/v1

Version of Record: A version of this preprint was published at Nature Nanotechnology on November 8th, 2021. See the published version at https://doi.org/10.1038/s41565-021-00999-w.

Abstract

The size tunability and chemical versatility of nanostructures provide attractive engineering potential to realize an electron source of high brightness and spatial temporal coherence, which is a characteristic ever pursued by high resolution electron microscopy. (1–3) Regardless of the intensive research efforts, electron sources that have ever produced atomic resolution images are still limited to the conventional field emitters based on a bulk W needle. It is due to the lack of fabrication precision for nanostructured sources, that is required to align a nanometric emission volume along a macroscopic emitter axis with sub-degree angular deviation. (4) In this work, we produced a LaB_6 nanowire electron source which was micro-engineered to ensure a highly collimated electron beam with perfect lateral and angular alignment. Such electron source was validated by installing in an aberration-corrected transmission electron microscope, where atomic resolution in both broad-beam and probe-forming modes were demonstrated at 60kV beam energy. The recorded un-monochromated 0.20eV electron energy loss spectroscopy (EELS) resolution, together with 20% probe forming efficiency and 0.4% probe current peak-to-peak noise ratio under a wide vacuum range, presented the unique advantages of nanotechnology and promised high performance low-cost electron beam instruments.

Introduction

Electrons emitted through electric field-induced tunneling are partially coherent in space and time. An electron source with high spatial temporal coherence is desired by applications of scanning electron microscope (SEM), transmission electron microscope (TEM) and scanning transmission electron microscope (STEM). To achieve high spatial coherence, electron emission volume is expected to be small; and to achieve high temporal coherence, the emission surface is expected with low work function. (5, 6) Conventional electrochemical etching technique is effective to produce nanoscale sharp needles out of refractory metals. Though it fulfills the small emission volume requirement, few work function options are available among this category of materials. W single crystal oriented along [310] lattice direction was a result of compromise and has been used as the high brightness electron source for electron microscopes that pursue the highest resolving power. (7, 8) This situation has not changed ever since the first atom-resolved STEM image was produced by Albert Crewe in 1970 using a W field emitter. (9) The concept of nanostructured electron source separates the material of support body and the material to emit electrons. While emitter support body could simply follow the conventional structure of a metal needle, the electron emitting unit could adopt nanostructures of various geometry and chemical composition. It became possible to tune independently both the emission volume and emission surface work function. Electron source-relevant nanostructures, to name a few, include: 0D atom clusters, 1D nanotube/nanowires (NW/NT), 2D nanosheets, high work function noble metal pyramids and negative electron affinity films. (2, 10-15) However, only few such nanostructured electron sources succeeded in producing SEM images of nanometer resolution and none has proven capable of atomic resolution imaging in TEM. (1, 16-18)

Angular alignment is one of the most important procedure to achieve high resolution imaging in electron microscopy. In a modern TEM column, electrons from emitter surface are expected to travel over 2 meters

in a straight line with nearly 0^o angular deviation. Even though sophisticated aligners were used in the column to steer electron beam, there is no angular adjustment mechanism available for the electron source in electron gun chamber, due to the difficulty of implementation at high voltage above ground. Therefore, in the electron source fabrication stage, emission direction must be pre-aligned along the emitter support body axis with sub-degree precision. Such nanomanipulation capability was not available to date.

In this work, a micro structure was fabricated on a support needle tip by focused ion beam (FIB); and a single LaB_6 nanowire was installed and aligned through SEM nanomanipulation. (19, 20) An angularly aligned emitter was validated in an aberration-corrected (S)TEM platform with a customized 60kV electron gun. Besides atomic imaging resolution, zero-loss peak (ZLP) energy resolution was also compared with that produced by a conventional W (310) electron gun using the same lens column and EELS spectrometer.

Main Text

Compared to other form of nanostructures, 1D NT/NW have been used the most extensively in electron source assemblies. (21) Its axial symmetry is compatible with an electron microscope column and its extended side surfaces provide sites for attaching to emitter support needle. (22) However, because of this side attachment configuration, axial symmetry of electric field distribution around the NT/NW tip could vanish. Such effect becomes more pronounced when short suspension length of NT/NW is used to reduce mechanical vibration. As a result, even though the NT/NW body is perfectly centered laterally and aligned angularly, the emitted electron beam will still be out of axis. To solve this problem, we used FIB to reshape the support needle tip into a collimator structure, as shown in the SEM image of figure 1a. The yellow pseudo color represents a collimator structure which is used to form axially symmetric electric field around the emission tip of a nanowire; Blue pseudo color represents a carbon pad that is used to stop chemical reaction between nanowire and metal support body during filament heating; Purple pseudo color represents the LaB_6 nanowire position. Height of the carbon pad is adjusted by FIB milling to ensure that the nanowire is positioned at the collimator center. Figure 1a inset is an optical microscope image of a TEM emitter showing an arch-shaped filament and the position of the fabricated microstructure at a Ta needle tip. The SEM snapshots of crucial steps of installing a LaB_6 nanowire into this microstructure are presented in figure 1b-d. In the first step, one LaB_6 nanowire was attached on a nanomanipulator hand through Van Der Waals force. Such nanowire was then transported through the collimator hole by driving the manipulator hand. (Figure 1b) After the nanowire got into full contact with the carbon pad, electron beam induced carbon deposition was applied to the bonding region to fix the nanowire. (Figure 1c) At the last step, manipulator hand was retracted and detached from the nanowire. It was realized because the Van Der Waals force is much weaker compared to carbon bonding force. (Figure 1d). Figure 1e and f showed a procedure where two manipulator hands are placed onto support needle at positions marked by two solid arrow heads. When the two manipulator hands moved in the direction of arrow heads, microscale bending of the support needle tip was realized. The bending amount was pre-determined by

measuring off-axis angle using field emission pattern, as shown in figure 1e inset. (1) In this case, even though the LaB_6 nanowire body (marked by a hollow arrow head) was already aligned with support needle axis, emission pattern still showed a 2.5-degree angle out of axis. Figure 1f is an SEM image of the emitter tip after 3-degree micro-bending performed by the two manipulator hands. Inset shows a perfectly aligned field emission spot on the phosphor screen center hole after such a set of manipulations.

In order to validate the above described LaB_6 NW emitter in a commercial TEM, a 60kV electron gun and high voltage tank were customized to adapt the changes in extraction voltage and total emission current. The extraction voltage and emission current for the LaB_6 nanowire emitter are ~400V and ~40nA, which are much lower than ~4000V and ~15uA, as used by conventional W (310) emitter. A TEM equipped with such a LaB_6 NW electron gun is shown in figure 2a. Components marked along beam path from top to bottom are the NW emitter, condenser lens aperture (CLA), specimen, high angle annular dark field (HAADF) detector, Faraday cage for probe current measurement, image screen, and EELS spectrometer. Figure 2b is a defocused TEM image about the CLA, taken after emitter centering with respect to the aperture using a gun motor capable of lateral movement. (23) Transmitted electrons and those scattered by the aperture edge form Fresnel diffraction fringes in the nearfield. The visibility of such fringes on the TEM screen is determined by an amplitude damping envelop formed due to lens aberration. Therefore, axially symmetric fringe pattern is observed only when the electron source is placed on the axis passing through the CLA center and thereby forming the same angles to the entire aperture edge circumference. Only a small portion of the total emitted electrons could go through the apertures and reach the image screen if emitter angular pre-alignment is poor. In this case of perfect pre-alignment, more than 10nA beam current could reach the image screen for low magnification TEM observation with large field of view. Figure 2c is a 30kx low-magnification TEM image showing a LaB_6 nanowire as synthesized by chemical-vapor-deposition method. Amplitude contrast is the main TEM image forming mechanism at this magnification. To demonstrate phase-contrast imaging, a Si [110] specimen was used to take high resolution TEM (HRTEM) images with magnifications from 400kx to 1000kx. A region from a 1000kx HRTEM image is displayed in figure 2d to show clear Si (111) planes. Figure 2e is a fast Fourier transform (FFT) diffractogram of the HRTEM image. (Sfigure1 in supplementary information) The highest observable spatial frequency corresponds to 90pm spacing of Si (442) planes. This spot is likely to be produced by secondary diffraction from two diffracted beams, because (442) is a forbidden reflection in primary diffraction pattern of diamond structure crystals. (24) The second smallest observable feature corresponds to 96pm of Si (440) planes. Two vectors were drawn in the diffractogram connecting the center transmitted spot to one 90pm spot and its neighboring 96pm spot respectively. The 96pm vector passes through Si (220) primary reflection and the 90pm vector passes through no primary reflections. Based on the principle of transmission cross-coefficient, non-linear phase contrast transfer function in the reciprocal space reaches maximum along primary reflection directions. (25, 26) High intensity damping occurs for secondary reflections that are out of those primary reflection directions, especially for high index reflections. If 96pm spot is also a secondary reflection, it would therefore be much brighter than 90pm spot as a result of higher phase contrast transfer. However, the fact that 96pm spot is weaker in

intensity compared to 90pm spot suggests that 96pm spot is a primary reflection which intensity is damped by lens aberration envelop. Therefore, an upper bound of information limit is estimated to be 96pm. Information limit of this TEM using the conventional W (310) emitter is 110pm~120pm. (27) The finer resolvable features by the LaB_6 NW electron source is a proof of higher spatial temporal coherence, which determines the damping envelop in a linear phase contrast transfer process. (28, 29)

It requires detailed knowledge of imaging condition and simulation to evaluate resolution quantitatively for an HRTEM image with spherical aberration. (30) STEM is a probe-forming mode of TEM. A demagnified image of the electron source forms an electron probe which is used to interact with specimen atom columns in raster scan manner. Image resolution can be directly measured by finding the smallest feature resolved in a STEM image. Figure 3a is a STEM image taken with HAADF detector about the Si [110] specimen, which is the same as that used for the TEM image of figure 2d. Each white dot in figure 2d is now resolved to be a dumbbell structure with 136pm atomic separation. The inset is a diffractogram of the image. The reflection with the highest observable spatial frequency is Si (440) with 96pm lattice spacing. Four Si atom columns marked by a red rectangle were magnified in figure 3b and their line profile is displayed below the image. The specimen thickness was determined to be 50nm by EELS method. (31) A multi-slice simulation at 60kV was then carried out by QSTEM to fit the image line profile with the assumption that the electron probe shape is a convolution between aberration-related broadening and a Gaussian shaped source image. (32, 33) The best fit was found when source image FWMH was set to be 60pm and it resulted in a probe shape with FWMH of 88pm. (Sfigure2 in supplementary information) Single atom imaging capability was demonstrated by STEM imaging of a single layer graphene specimen, which is presented in figure 3c. Three pairs of graphite (200) reflections with 107pm spacing were clearly shown in figure 3d, which is a diffractogram of figure 3c. Four neighboring C atoms in figure 3c as selected by a red rectangle were used to make a line profile shown in figure 3e. The same electron probe with 88pm FWHM was again used to simulate a graphene image. The well-matched line profile thereby verified our previous probe size estimation.

To take advantage of the high current stability of the LaB_6 nanowire emitter in moderate UHV condition, our customized electron gun was only pumped by ion pumps to keep vacuum in the ~10^{-8}Pa range, while the original W (310) electron gun vacuum was in the ~10^{-10}Pa range enhanced by non-evaporable getter pumps. (34) As figure 4a shows, 21% of total emission current from a LaB_6 nanowire emitter could be used as probe current, which is measured using a Faraday cage near the image screen. Low noise level in the probe current is especially important for single atom HAADF imaging of low atomic weight elements because of their small electron scattering cross-section. In the case of graphene, signal-to-noise ratio is typically ~10%. (35) To allow 8-bit greyscale information, the noise level of STEM probe current is expected to be below 0.4%. Figure 4b is the probe current profile measured for 1 minute, which is longer than the usual STEM frame acquisition time. A peak-to-peak noise ratio of 0.36% was demonstrated, even after a full day of use without emitter heat treatment. EELS is an indispensable spectroscopy method that has become standard to combine with STEM to realize atomic resolution chemical analysis. (36) While its spatial resolution depends on STEM probe size, its energy resolution depends on probe temporal

coherence, which can be measured as the FWHM of ZLP. Electron probe energy spread originated from emitter energy spread and column related factors such as instability of high voltage tank, objective lens and EELS spectrometer, all contribute to the final measured ZLP width. To compare the ZLP between LaB_6 NW electron gun and W (310) electron gun on equal ground, we acquired ZLPs from both electron guns using the same column, spectrometer and high voltage tanks with negligible noise compared to the expected energy spread range. Figure 4c includes ZLPs from LaB_6 NW emitter, W (310) emitter and Schottky emitter all acquired at 60kV acceleration voltage and ~15pA probe current. 0.22eV, 0.28eV and 0.8eV were measured as FWHMs for the three electron guns respectively. ZLP FWHMs with respect to probe current were also plotted for both the LaB_6 NW electron gun and W (310) electron gun in figure 4d. At probe current ~5pA, both electron guns reached the narrowest ZLPs which are 0.2eV and 0.27eV respectively. (Sfigure3 in supplementary information) It is noted that the LaB_6 nanowire electron gun energy spread is consistent with our previous measurement using hemispherical analyzer in a low voltage field emission chamber. (1) However, energy spread from W (310) emitter was much higher in our previous measurement. It is due to the >100-fold higher vacuum in the JEM-Arm200F TEM electron gun where W (310) could maintain a clean surface for a much longer time. On the other hand, the less vacuum stringency and consistent performance of LaB_6 nanowire emitter in a wide range of vacuum conditions make it suitable for applications in various electron microscopes of a wide cost range. (37, 38)

As a conclusion, micro-fabrication and nano-manipulation were carried out to make perfectly angularly aligned LaB_6 NW electron source. Such an electron source was installed in an aberration-corrected (S)TEM where sub-angstrom features in both broad-beam mode and probe-forming mode were resolved at 60kV acceleration voltage. The higher spatial temporal coherence offered by the nanostructured electron source produced advantages over the state-of-the art W (310) electron source in both microscopic spatial resolution and spectroscopic energy resolution. With the additional merits of low vacuum stringency and probe-forming efficiency from the LaB_6 NW electron source, a natural next step would be applying such emitter in high voltage monochromated (S)TEM applications to benefit frontier studies such as atomic resolution vibrational spectroscopy. (39, 40) Another development direction would be a new generation low-cost electron beam imaging and chemical analysis instruments with not only high performance but also broader applicability and affordability.

Declarations

Acknowledgements

This study was supported by NIMS Advanced Measurement and Characterization Project.

Author contributions

HZ carried out the experiments and wrote the manuscript. YJ and AN carried out physical evaluation of LaB_6 nanowire emitter with TEM. AI developed high voltage electronics for LaB_6 nanowire emitter electron gun. AY acquired STEM and TEM data. OC and KK contributed in (S)TEM image analysis and simulation.

TK, HTM and HW carried out nanomanipulation. NT contributed in nanowire synthesis. YY, DF, SK, and HM coordinated the project.

Competing interests

The authors declare no conflict interests for this work.

Additional information

Supplementary information is available.

References

1. Zhang, H., Tang, J., Yuan, J., Yamauchi, Y., Suzuki, T., Shinya, N., Nakajima, K., Qin, L. An ultrabright and monochromatic electron point source made of a LaB_6 Nature Nanotechnology. 11, 3 (2016) 273-279
2. De Jonge, N., Lamy, Y., Schoots, K., Oosterkamp, T. High brightness electron beam from a multi-walled carbon nanotube. Nature 420 (2002) 393-395;
3. Williams, D., Carter, C., Transmission electron microscopy: a textbook for materials science, Vol. 1 (Springer, 2009);
4. Swanson, L., Schwind, G. A review of the cold-field electron cathode. Adv. Imaging Electron Phys. 159, (2009) 63–100;
5. Fink, H., Stocker, W., Schmid, H. Holography with low-energy electrons, Phys. Rev. Lett. 65, 10 (1990) 1204-1206;
6. Gadzuk, J., Plummer, E. Field emission energy distribution (FEED) Rev. Mod. Phys. 45, 3 (1973) 487-548;
7. Krivanek, O., Chisholm, M., Nicolosi, V., Pennycook, T., Corbin, G., Dellby, N., Murfitt, M., Own, C., Szilagyi, Z., Oxley, M., Pantelides, S., Pennycook, S. Atom-by-atom structural and chemical analysis by annular dark-field electron microscopy, Nature 464 (2010) 571-574;
8. Haruta, M., Kurata, H. Direct observation of crystal defects in an organic molecular crystals of copper hexachlorophthalocyanine by STEM-EELS, Sci. Rep. 2 (2012) 252;
9. Crewe, A., Wall, J., Langmore, J. Visibility of single atoms, Science 168 (1970) 1338-1340;
10. Chang, C., Kuo, H., Hwang, I., Tsong, T. A fully coherent electron beam from a noble-metal covered W(111) single-atom emitter. Nanotechnology 20, 11 (2009) 115401;
11. Binh, V., Purcell, S., Garcia, N., Doglioni, J. Field emission electron spectroscopy of single-atom tips. Phys. Rev. Lett. 69, 17 (1992) 2527-2530;
12. Shao, X., Srinivasan, A., Ang, W., Khursheed, A. A high-brightness large-diameter graphene coated point cathode field emission electron source. Nat. Comm.. 9 (2018) 1288;

13. Diehl, R., Choueib, M., Choubak, S., Martel, R., Perisanu, S., Ayari, A., Vincent, P., Purcell, S. T., Poncharal, P. Narrow energy distributions of electrons emitted from clean graphene edges. Phys. Rev. B, 102 (2020) 035416;
14. Hwang, I., Kuo, H., Chang, C., Tsong, T. Noble-metal covered W(111) single-atom electron sources. ECS Transactions 25, 10 (2009) 3-18;
15. Tafel, A., Meier, S., Ristein, J., Hommelhoff, P. Femtosecond laser-induced electron emission from nanodiamond-coated tungsten needle tips. Phys. Rev. Lett. 123, 14 (2019) 146802;
16. Suga, H., Abe, H., Tanaka, M., Shimizu, T., Ohno, T., Nishioka, Y., Tokumoto H. Stable multiwalled carbon nanotube electron emitter operating in low vacuum, Surf. Interface Anal. 38 (2006) 1763-1767;
17. Nakahara, H., Ichikawa, S., Ochiai, T., Kusano, Y., Saito, Y. Carbon nanotube electron source for field emission scanning electron microscopy, e-J. Surf. Sci. Nanotech. 9 (2011) 400-403;
18. Mamishin, S., Kubo, Y., Cours, R., Monthioux, M., Houdellier, F. 200keV cold field emission source using carbon cone nanotip: application to scanning transmission electron microscopy. Ultramicroscopy. 182 (2017) 303-307;
19. Miyazaki, H.T., Miyazaki, H., Ohtaka, K., & Sato, T. Photonic band in two-dimensional lattices of micrometer-sized spheres mechanically arranged under a scanning electron microscope. J. Appl. Phys. 87 (2000) 7152–7158;
20. Aoki, K., Miyazaki, H.T., Hirayama, H., Inoshita, K., Baba, T., Sakoda, K., Shinya, N., and Aoyagi, Y. Microassembly of semiconductor three-dimensional photonic crystals. Nat. Mater. 2 (2003) 117-121;
21. Zhang, H., Tang, J., Yuan, J., Qin, L.C. Ultrabright and monochromatic nanowire electron sources. MRS Bulletin. 42, 7 (2017) 511-517;
22. Zhao, P., Zhang, Y., Tang, S., Zhan, R., She, J., Chen, J., Deng, S. A universal method to weld individual one-dimensional nanostructures with a tungsten needle based on synergy of the electron beam and electrical current, Nanomaterials 10 (2020) 469;
23. Houdellier, F., Masseboeuf, A., Monthioux, M., Hytch, M. New carbon cone nanotip for use in a highly coherent cold field emission electron microscope. Carbon. 50 (2012) 2037-2044;
24. Warren, B., X-ray diffraction, (Dover publications, 2012);
25. Ishizuka, K. Contrast transfer of crystal images in TEM, Ultramicroscopy 5 (1980) 55-65;
26. O'Keefe, M. "Resolution" in high-resolution electron microscopy, Ultramicroscopy 47 (1992) 282-297;
27. JEM-ARM200F NEOARM Atomic Resolution Analytical Electron Microscope specification: https://www.jeol.co.jp/en/products/detail/JEM-ARM200F_NEOARM.html
28. Kimoto, K., Sawada, H., Sasaki, T., Sato, Y., Nagai, T., Ohwada, M., Suenaga, K., Ishizuka, K. Quantitative evaluation of temporal partial coherence using 3D Fourier transforms of through-focus TEM images, Ultramicroscopy 134 (2013) 86-93;
29. Morishita, S., Mukai, M., Suenaga, K., Sawada, H., Resolution enhancement in transmission electron microscopy with 60-kV monochromated electron source, Appl. Phys. Lett. 108 (2016) 013107;

30. Kimoto, K., Kurashima, K., Nagai, T., Ohwada, M., Ishizuka, K. Assessment of lower-voltage TEM performance using 3D Fourier transform of through-focus series, Ultramicroscopy 121 (2012) 31-37;
31. Malis, T., Cheng, S. C., Egerton, R. F. EELS log-ratio technique for specimen-thickness measurement in the TEM, J. Electron Microscope Technique 8 (1988) 193;
32. Koch, C. T. Determination of Core Structure Periodicity and Point Defect Density along Dislocations, Physics, Arizona State University, 2002, p. 175.
33. Sasaki, T., Sawada, H., Okunishi, E., Hosokawa, F., Kaneyama, T., Kondo, Y., Kimoto, K., Suenaga, K. Evaluation of probe size in STEM imaging at 30 and 60kV, Micron 43 (2012) 551-556;
34. Kasuya, K., Katagiri, S. & Ohshima, T. Stabilization of a tungsten <310> cold field emitter. J. Vac. Sci. Technol. B 28 (2010) L55–L60;
35. Yamashita, S., Koshiya, S., Nagai, T., Kikkawa, J., Ishizuka, K., Kimoto, K. Quantitative annular dark-field imaging of single-layer graphene-II: atomic-resolution image contrast, Microscopy (2015) 409-418;
36. Kimoto, K., Asaka, T., Nagai, T., Saito, M., Matsui, Y., Ishizuka, K. Element-selective imaging of atomic columns in a crystal using STEM and EELS, Nature 450 (2007) 702-704;
37. Kasuya, K, Kusunoki, T., Hashizume, T., Ohshima, T., Katagiri, S., Sakai, Y., Arai, N.. Monochromatic electron emission from CeB6 (310) cold field emitter. Appl. Phys. Lett. 117 (2020) 213103;
38. Kusunoki, T., Hashizume, T., Kasuya, K, Arai, N.. Stabilization of cold-field-emission current from a CeB6 single-crystal emitter by using a faceted (100) plane, J. Vac. Sci. Technol. B 39 (2021) 013202;
39. Krivanek, O., Lovejoy, T., Dellby, N., Aoki, T., Carpenter, R., Rez, P., Soignard, E., Zhu, J., Batson, P., Lagos, M., Egerton, R., Crozier, P. Vibrational spectroscopy in the electron microscope, Nature 514 (2014) 209-212;
40. Hage, F., Radtke, G., Kepaptsoglou, D., Lazzeri, M., Ramasse, Q. Single-atom vibrational spectroscopy in the scanning transmission electron microscope, Science 367 (2020) 1124-1127.

Methods

The LaB_6 NW electron gun was first installed on an experimental JEM-2200FS TEM to confirm emitter alignment, emission stability and low magnification imaging. After that, it was transported and mounted on a JEM-Arm200F (S)TEM, which is equipped with a UHR objective pole piece and a probe-forming CEOS ASCOR spherical aberration corrector. LaB_6 nanowire electron gun was constructed with 2-anode structure. The first anode A1 provides extraction field to determine total emission current and the second anode A2 controls beam current that comes out of electron gun exit. Under imaging condition of this work, total emission current was kept at 40nA while electron gun demagnification was adjusted by varying A2 voltage. Electromagnetic sensors were not equipped with this experimental electron gun. During STEM image acquisition, demagnification ratio was adjusted to minimize image distortion caused by stray electromagnetic field interference. For STEM imaging, CLA size, beam semi-convergence angle, inner and outer detector angles, probe current are 50um, 38.5mrad, 48mrad, 200mrad, 1.7pA respectively.

Images are formed by either using a short dwell time of 5us with 20 scans accumulation or a long dwell time of 20us with single scan. Exposure time of 0.5s was used for TEM image acquisition. GIF-quantum ER was used for EELS spectrum acquisition. CLA size, camera length, spectrometer dispersion, entrance aperture size, exposure time are 50um, 2.5cm, 0.01eV/Channel, 2.5um, 0.01s, respectively.

Figures

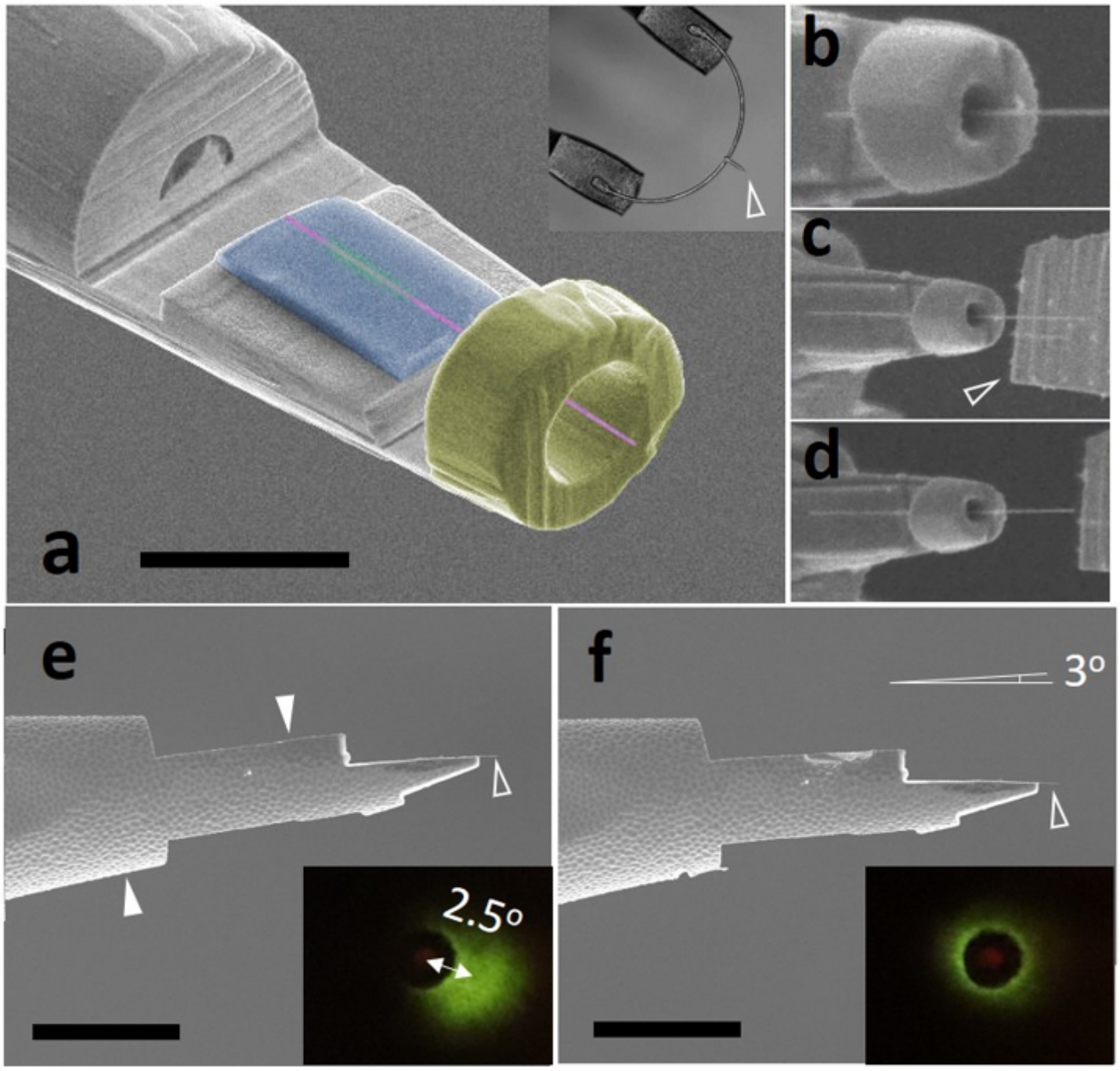

Figure 1

Micro-engineering of nanowire electron source. (a) A pseudo-color SEM image of a LaB6 nanowire electron source. Yellow, blue, purple, green colors represent tip collimator, carbon pad, nanowire position and carbon bonding layer, respectively. Inset being a TEM nanowire emitter with W arch filament and a Ta support needle. Scale bar: 5um; (b-d) Fabrication procedure snapshots of a nanowire going through the tip collimator (b), being attached to carbon pad (c), and released from manipulator hand (d); (e) A nanowire emitter before angular adjustment. Inset being a field emission pattern showing 2.5o mis-alignment angle; (f) Same emitter after angular adjustment through tip micro-bending. Scale bar in (e) and (f): 15um.

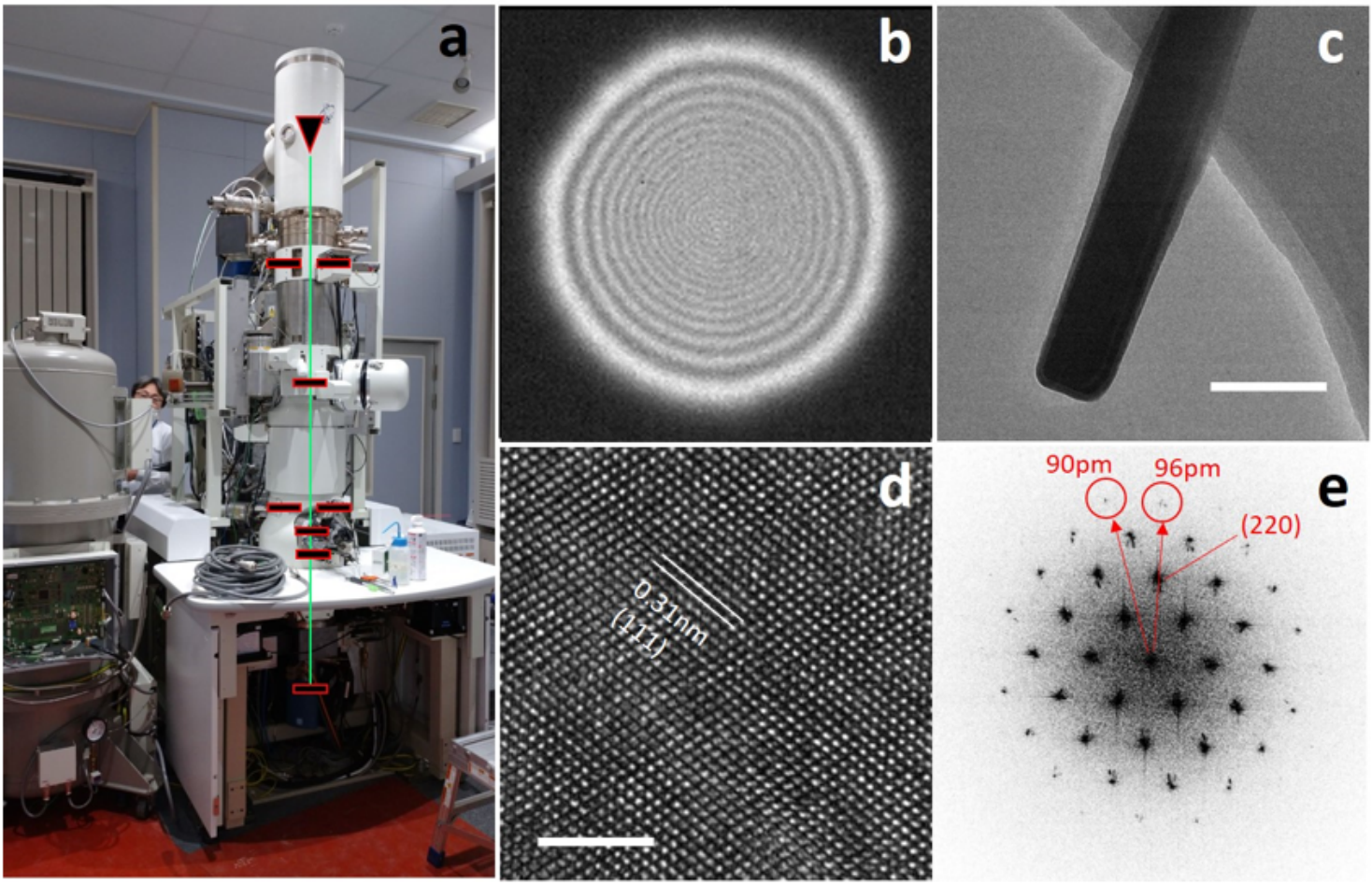

Figure 2

Coherent TEM imaging using LaB6 nanowire electron gun. (a) Structure of the LaB6 nanowire TEM. Components labelled along beam path from top to bottom: nanowire emitter, condenser lens aperture, specimen, annular dark field detector, Faraday cage, image screen, and EELS spectrometer; (b) Fresnel diffraction pattern formed around condenser lens aperture imaged at defocus condition after emitter centering; (c) 30kx low magnification TEM image of a LaB6 nanowire on holey carbon. Scale bar: 100nm; (d) 1000kx high resolution TEM image of Si along [110] lattice direction. Scale bar: 4nm; (e) Fast Fourier transform diffractogram showing the highest spatial frequency reflection of 90pm.

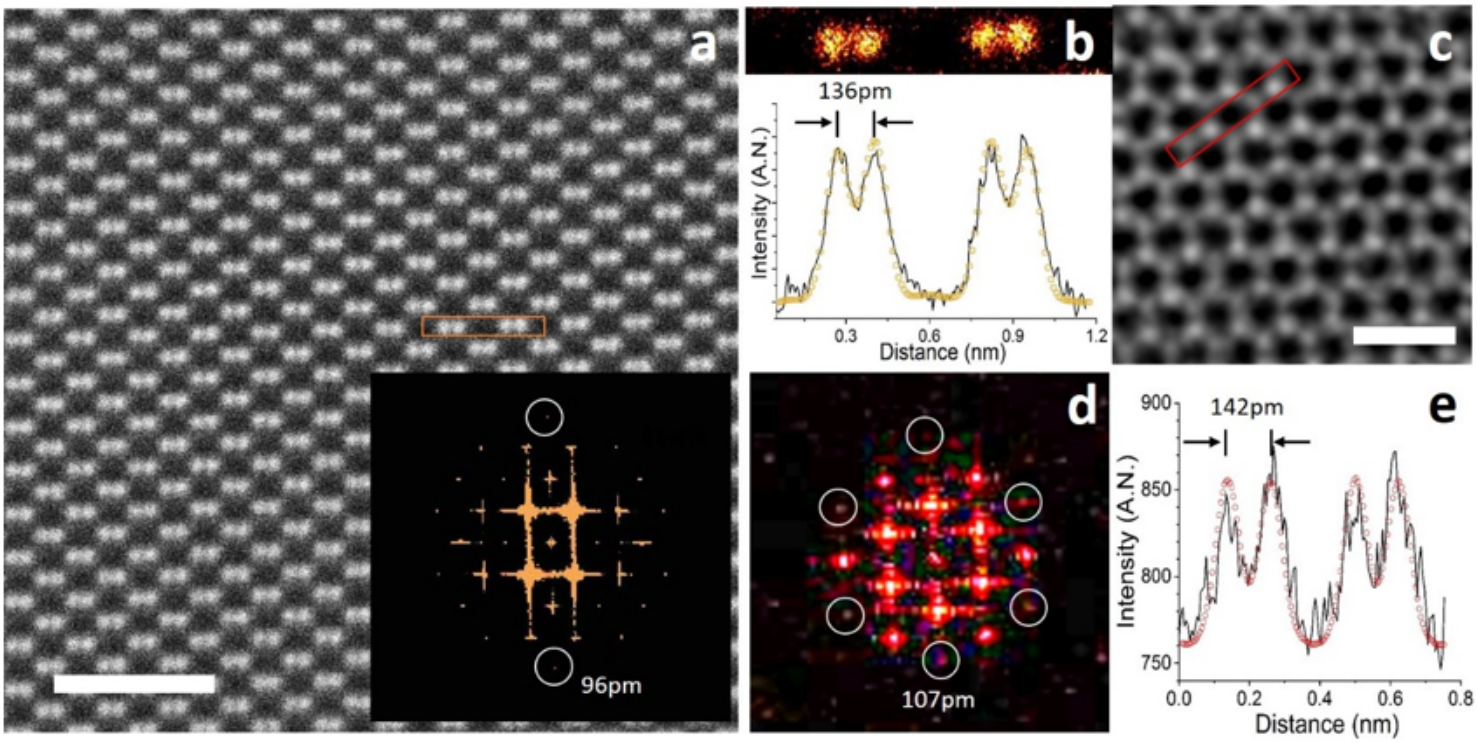

Figure 3

Aberration-corrected STEM imaging using LaB6 nanowire electron gun. (a) HAADF STEM raw image showing Si dumbbell structures along [110] lattice direction. Scale bar: 2nm. Inset: FFT diffractogram showing 96pm resolution; (b) Magnified image of two Si dumbbells from the region marked by a yellow rectangle in (a). Below: its line profile (black line) fitted with simulation which assumes a Gaussian source shape (yellow circles); (c) HAADF STEM image of a single layer graphene after gaussian-blur filter. Scale bar: 1nm; (d) diffractogram of (c) showing 107pm resolution in single atom imaging; (e) Line profile of 4 C atoms in (c) (black line) and simulated profile using the same probe shape as in (b) (red circles).

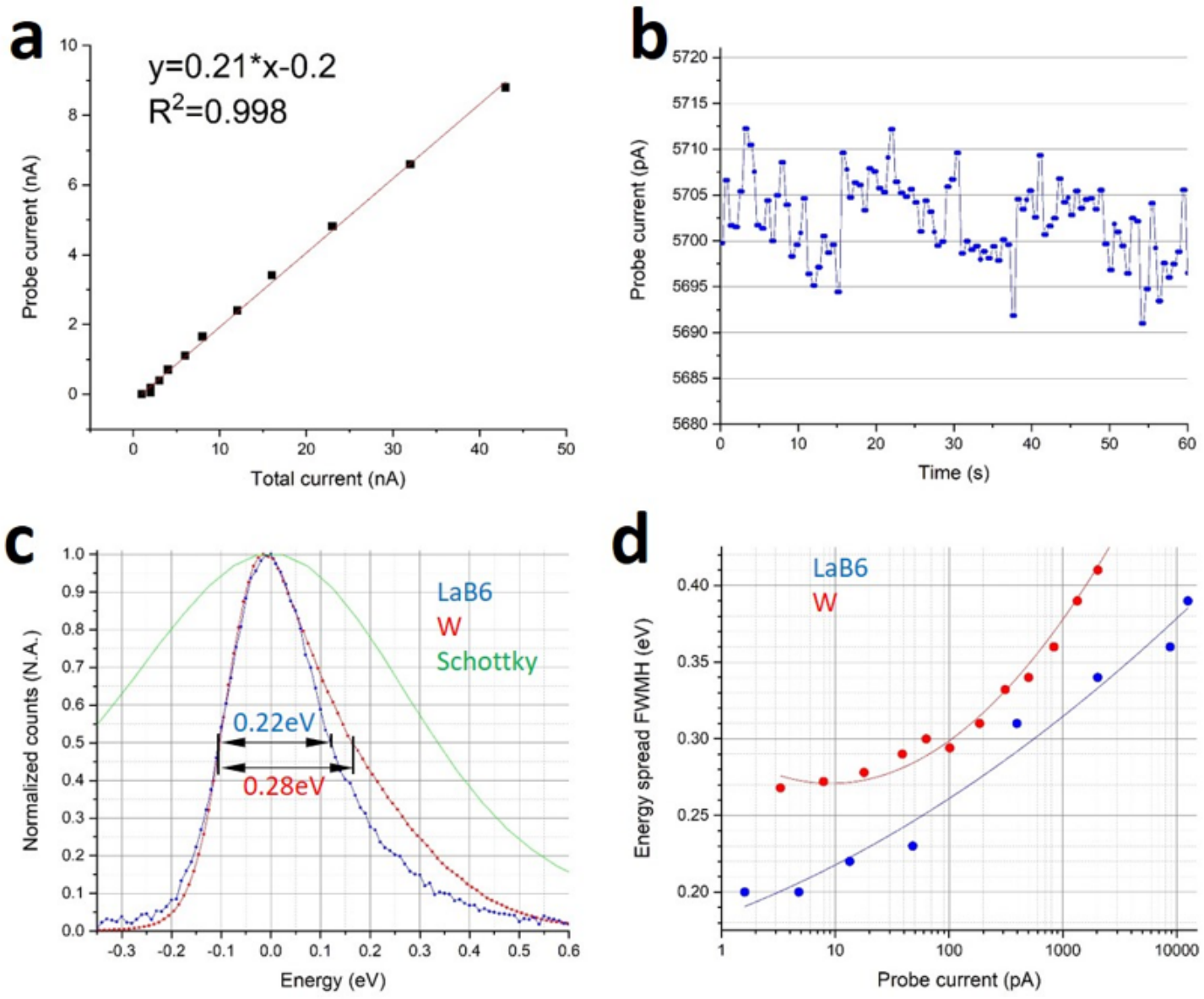

Figure 4

Un-monochromated EELS energy resolution. (a) Electron probe-forming efficiency of the LaB6 nanowire emitter with respect to total emission current; (b) Short-term stability of probe current generated by the LaB6 nanowire electron gun; (c) Zero loss peaks of EELS measured at ~15pA for LaB6 nanowire emitter, W(310) emitter and Schottky emitter, respectively; (d) FWHM energy spread measured at a range of probe current for LaB6 nanowire electron gun and W (310) electron gun.

Supplementary Files

This is a list of supplementary files associated with this preprint. Click to download.

- Supplementary210421.docx